Photochemical & Photobiological Sciences (2021) 20:255–263
https://doi.org/10.1007/s43630-021-00014-0

ORIGINAL PAPERS

Fe(III)-polyuronic acid photochemistry: radical chemistry in natural polysaccharide

M. H. Jayan S. Karunarathna[1] · Mayokun J. Ayodele[1] · Giuseppe E. Giammanco[1] · Alexander M. Brugh[1] · Dayana A. Muizzi[1] · Mariia A. Bauman[1] · Andrew T. Torelli[1,3] · Anginelle M. Alabanza[2] · Malcolm D. E. Forbes[1,2] · Alexis D. Ostrowski[1]

Received: 9 October 2020 / Accepted: 19 January 2021 / Published online: 11 February 2021
© The Author(s), under exclusive licence to European Photochemistry Association,European Society for Photobiology 2021

Abstract

The photochemistry of Fe(III) coordinated to natural uronate-containing polysaccharides has been investigated quantitatively in aqueous solution. It is demonstrated that the photoreduction of the coordinated Fe(III) to Fe(II) and oxidative decarboxylation occurs in a variety of uronate-containing polysaccharides. The photochemistry of the Fe(III)-polyuronic acid system generated a radical species during the reaction which was studied using the spin trapping technique. The identity of the radical species from this reaction was confirmed as $CO_2^{\bullet-}$ indicating that both bond cleavage of the carboxylate and oxidative decarboxylation after ligand to metal charge transfer radical reactions may be taking place upon irradiation. Degradation of the polyuronic acid chain was investigated with dynamic light scattering, showing a decrease in the hydrodynamic radius of the polymer assemblies in solution after light irradiation that correlates with the Fe(II) generation. A decrease in viscosity of Fe(IIII)-alginate after light irradiation was also observed. Additionally, the photochemical reaction was investigated in plant root tissue (parsnip) demonstrating that Fe(III) coordination in these natural materials leads to photoreactivity that degrades the pectin component. These results highlight that this Fe(III)-polyuronic acid can occur in many natural systems and may play a role in biogeochemical cycling of iron and ferrous iron generation in plants with significant polyuronic acid content.

Graphic abstract

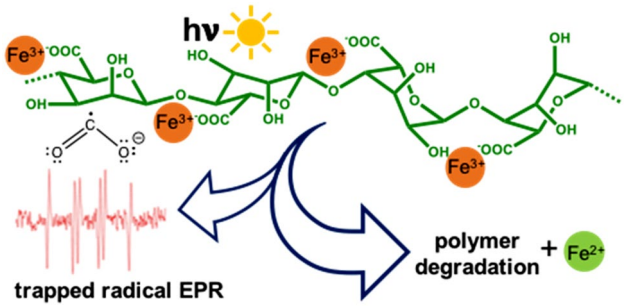

Keywords Iron photochemistry · Polysaccharides · Carbon radicals · Biogeochemical iron cycling · Bioinorganic photochemistry

Abbreviations

Pect	Pectate
AlgG	Alginate G (35% mannuronate)
AlgI	Alginate I (61% mannuronate)
AlgM	Alginate M (65% mannuronate)
NA	Noni
Xant	Xanthan Gum

✉ Malcolm D. E. Forbes
forbesm@bgsu.edu

✉ Alexis D. Ostrowski
alexiso@bgsu.edu

Extended author information available on the last page of the article

OS	Oxidized Starch
HA	Hyaluronic Acid
GA	Gum Arabic
NMR	Nuclear magnetic resonance
QY	Quantum yield
EPR	Electron paramagnetic resonance
SEM	Scanning electron microscopy
EDTA	Ethylenediaminetetraacetic acid
Mw	Molecular weight
LED	Light emitting diode

1 Introduction

The coordination of Fe(III) occurs in a variety of natural systems, and perhaps the most well-known Fe(III) coordinating species are siderophores [1, 2]. Certain siderophores employ α-hydroxy acid groups that strongly coordinate a single Fe(III) ion [3, 4]. Alternatively, some marine plants also coordinate Fe(III), though Fe(III) coordination in giant kelp (*Macrocystis pyrifera*), and brown algae (*Ectocarpus siliculosus*) is achieved via carboxylate containing polysaccharides (polyuronates) [5, 6]. The photochemistry of Fe(III)-carboxylates has been widely described for a number of natural systems, including siderophores [1–3, 7] and complexes of Fe(III) with small molecules like citrate or oxalate [8–14], and the photochemistry is known to impact many biogeochemical processes [15–18]. The photoreactivity of the Fe(III)-coordination complexes is possible due to their favorable optical properties, presenting a ligand-to-metal charge transfer (LMCT) absorption band at a relatively low energy (i.e. in the UV–visible region) which in turn allows access to non-luminescent, short-lived, and highly reactive excited states [12, 19–21].

It is well documented that the photoreduction of Fe(III)-α-hydroxy acids primarily leads to the generation of organic radical species which is consequently followed by a rapid decarboxylation process [8, 11, 13, 20, 20–24]. The decarboxylation step may lead to the formation of either carbon-centered radicals (CCR) or carbon (IV) oxide anion radical which are both often short-lived (Scheme 1). We have also now reported the photoreactivity of Fe(III)-polyuronate hydrogels [19], which mimic the coordination of Fe(III) in macroalgae *Macrocystis pyrifera* and *Ectocarpus siliculosus*, [25] and show similar photochemistry to the α-hydroxy acids. To the best of our knowledge, there are no reports on the structural characterization of the radicals generated via Fe(III)-polyuronate photochemistry, for example using electron paramagnetic resonance (EPR) spectroscopy.

In this paper we apply the spin trapping technique to track these reactions using the common nitrone spin trap 5,5-dimethyl-1-pyrroline N-oxide (DMPO). The spin trapping reaction is typically used when radicals are too short lived or not produced in a high enough concentration to be observed directly by EPR. The reaction can be run for some time to build up stable spin adducts created when the radical of interest adds across the double bond of the nitrone (Scheme 2). This allows us to interrogate the generated radicals, and confirm the photochemical pathway in the Fe(III)-polyuronate system. We also show the scope of the photoreaction, characterizing the photochemistry for many different Fe(III)-polyuronic acids.

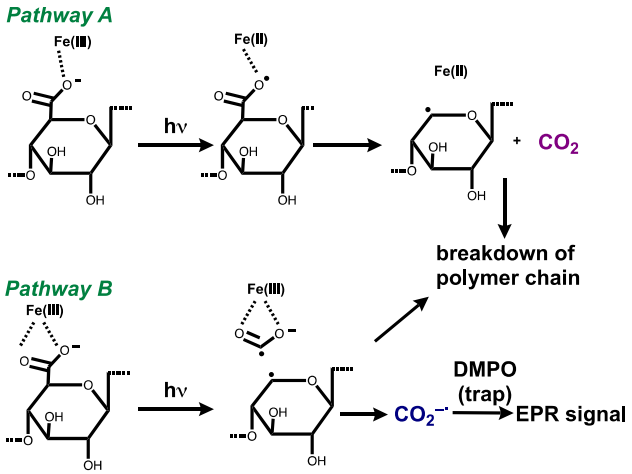

Scheme 1 Photolysis of Iron(III) in the presence of polyuronates generates a radical

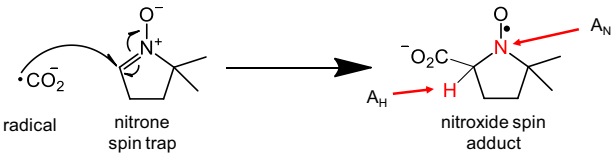

Scheme 2 Example of a generic radical (R) reacting with DMPO to produce a stable nitroxide. The atoms responsible for hyperfine splitting AN and AH are indicated

These results will provide information on how the photoactive Fe(III)-polyuronates are playing a role in biogeochemical cycling of iron and generation of bioavailable Fe(II). Fe(III)-polyuronic acids have been shown to play a role in iron uptake in plants, [26, 27] This could uncover a new role for Fe(III)-carboxylate photochemistry in other natural systems, and implicate plants as important participants in photochemical iron cycling as well.

2 Experimental

2.1 Materials

Low viscosity sodium alginate from brown algae (AlgM, Mw 45,000 g/mol) (Lot A112), Pectin from citrus peel

with 74% galacturonic acid (Lot SLBN9007V Mw 25,000–50,000), Gum Arabic from acacia tree Mw 250,00, 2,2,6,6–Tetramethylpiperidin-1-oxyl (TEMPO) 98%, Sodium chlorite, Ferric chloride hexahydrate 99%, morpholine (99%) and 5,5-Dimethyl-1-pyrroline N-oxide 97% (DMPO), were all purchased from Sigma-Aldrich and used as received. Only freshly prepared solutions of Fe(III) chloride were used to ensure minimal precipitation of iron oxides/hydroxides. Medium viscosity alginate (AlgI) and high-guluronate alginate (AlgG), product codes IL-6F and IL-6G respectively, were kindly supplied by Kimica Corporation, Japan (Mw 97,000). Poly-D-galacturonic acid 95%, Mw 25,000–50,000 g/mol (Lot. 81325) was purchased from Sigma-Aldrich and prepared as the sodium salt by neutralization with NaOH. This material is referred to as "pectate". Hyaluronic acid sodium salt from Streptococcus equi, (Mw 1,500,000–1,800,000 g/mol) was purchased from either Sigma-Aldrich or Acros. Soluble potato starch and Hydroxylamine hydrochloride were used as received from Mallinckrodt. Xanthan Gum (Mw 1,800,000–3,600,000) was purchased from Now Foods and used as received. Noni fruits (Morinda citrifolia) were harvested when slightly soft, from Wai'anae, Hawaii in April 2015 and stored at − 18 °C until extraction of the polysaccharide. Sodium hypochlorite (10–13% chlorine content) and 1,10 Phenanthroline (99% pure) were used from Aldrich chemical company. Ethanol (200 proof) was purchased from Pharmco-Aaper. Acetone, Methanol and Sodium Hydroxide were purchased from EMD Millipore corporation 99% pure. Deuterated dichloromethane was purchase from Cambridge (99% pure) and was used as received.

2.2 Methods

2.2.1 Electron paramagnetic resonance (EPR)

Aqueous samples of the Fe(III)-polyuronates with DMPO were prepared in the dark in a 1:5 molar ratio respectively. The concentration of the solution is a 0.9 mM Fe(III) and 1% by weight polyuronate. Photo-integrity of samples were preserved after preparation by wrapping sample vials securely with aluminum foil. Samples were then taken immediately for analysis with EPR. A 0.1 mL aliquot of sample was bubbled with N_2 for 15 min placed in a quartz capillary and air sealed. The capillary tube was then inserted into a TE011 resonant cavity of the EPR machine. A JEOL JES-X3 spectrometer connected with an X-band (9.5 GHz) microwave bridge and 100 kHz modulation was used to carry out steady state experiments under ambient conditions. All experiments were conducted scanning over a sweep of 15 mT with modulation amplitude set to 0.1 mT. EPR spectra were recorded at different time intervals upon photolysis with a 405 nm LED light source coupled to the cavity. Spectra were simulated using Easyspin [28] from which the hyperfine coupling constant of the nitrogen nucleus (A_N) and β-protons ($A_{H\beta}$) were obtained.

2.2.2 Irradiation

All irradiation was performed with a ThorLabs 405 nm LED light source with light intensity 50 mW cm^{-2} unless stated otherwise.

2.2.3 Synthesis of partially oxidized starch (OS)

Potato starch, 1 g, was suspended in 100 mL deionized water and gelatinized at 90–95 °C. Next, the solution was cooled down to 20 °C before adding 10 mg TEMPO and 390 mg KBr. The pH was adjusted to 10.7 with 6 M NaOH. Then, the NaOCl solution (45 mL, 10–13% chlorine) was added drop wise in a 60 min period to the starch/TEMPO solution. While the hypochlorite was added, the pH was constantly measured and adjusted to 10.7 by the dropwise addition of 0.5 M NaOH. Finally, the solution was neutralized with HCl and the reaction quenched by adding 10 mL ethanol. The product was precipitated with methanol, centrifuged and lyophilized. A degree of oxidation of 82% was calculated for the ratio of areas of the 1H NMR peaks at 4.60 and 4.40 ppm, corresponding to the anomeric proton H–C [1] of glucuronic acid and anhydroglucose, respectively.

2.2.4 Extraction of noni polysaccharide

The purification of the polysaccharide from Noni (Morinda citrifolia) was performed following a reported procedure [29]. Briefly, ripened noni fruits were strained to separate the pulp from the seeds. Then, fruit juices were centrifuged, and any pulp was discarded. The polysaccharide was precipitated from this aqueous juice solution by the addition of 4 volumes of 200 proof ethyl alcohol and further centrifuged (Thermo Scientifc Sorvall Biofuge Primo centrifuge Rpm 3000 for 3 min). The supernatant was discarded, and the white solid was again dissolved in minimum amount of de-ionized water to re-dissolve the white solid. This precipitation process was repeated two more times (addition of ethanol and centrifugation) before lyophilizing the final white product. The yield of noni polysaccharide was 0.3% by mass of the seedless pulp. The polysaccharide isolation was confirmed by NMR (Fig. S1).

2.2.5 Photochemistry of Fe(III)-polysaccharides

The photo-chemical study of the Fe(III)-polysaccharides was based on a method reported previously [19]. Briefly, solutions of the polysaccharide were prepared in deionized water

and mixed with $FeCl_3$ solutions to achieve a final concentration of 1% by weight in the polysaccharide, and 0.9 mM Fe(III). Since some solutions were too viscous under these conditions, we also prepared samples that were 0.25% by weight of the polysaccharide and 0.225 mM in Fe(III). Samples were irradiated in 1 cm quartz cuvettes equipped with a magnetic stirrer under air atmosphere, at room temperature. The quantum yield (Φ, QY) for each system was determined by measuring the moles of Fe(III) reduced to Fe(II) per mol of photons absorbed by the sample (Eq. 1).

$$\phi_{\mathrm{Fe(II)}} = \frac{n\mathrm{Fe(II)}}{I_0\left(1-10^{-\mathrm{Abs}}\right)} \quad (1)$$

where *n*Fe(II) is the moles of ferrous iron produced during the photoreaction, determined by recording the absorbance of a 1,10-phenathroline complex at 510 nm; I_0 is the moles of photons hitting the sample as determined by ferrioxalate actinometry ($I_0 = 3.7 \times 10^{-8}$ Einsteins/s), [30] and Abs is the optical density of the sample at the irradiation wavelength (405 nm).

2.2.6 Dynamic light scattering

For these experiments 0.25% by weight polysaccharide solutions with a 0.225 M concentration of Fe(III) were prepared by slowly mixing previously filtered (0.2 µm syringe filter) solutions of the polysaccharide and metal ion. Aliquots (2 mL) were irradiated for increasing periods of time at 405 nm (50 mW cm^{-2}) under constant stirring. Then, 100 µL aliquots of the irradiated sample were diluted to a final volume of 1 mL and the samples were analyzed by dynamic light scattering. Measurements were performed using a Nanostar dynamic light scattering instrument (Wyatt Technology). A total of 10 scans were recorded per measurement, and measurements were obtained in triplicate for each sample.

2.2.7 Circular dichroism

CD spectra for alginates were recorded as previously reported [19]. In brief, 0.8 mg/mL alginate solutions were prepared using DI water and the readings were collected every 0.5 nm with an integration time of 1 s using an AVIV 62DS circular dichroism spectrophotometer at 25 °C (Fig. S2) and percent mannuronate (%M) in alginate was calculated based on a previously reported method [31].

2.2.8 Viscosity determination with oscillatory rheology

Alginate solutions of 1% by weight were used for the viscosity measurements. TA Instruments Discovery HR-2 rheometer with a 50 mm parallel plate geometry was used on flow sweep mode at 25 °C. The viscosity was measured with the change of shear rate from 1 to 1000 s^{-1} and the linear range for the viscosity between 10 and 100 s^{-1} regions was averaged to obtain the viscosity. A $FeCl_3$ solution with 0.9 mM concentration was prepared and alginate was dissolved in 1% by weight. Irradiations were performed using a 405 nm LED source at 50 mW cm^{-2} power for different time intervals and the change in viscosity was measured using the same conditions mentioned above.

2.2.9 Modulus determination of parsnip root tissue

Parsnip was cut into 2 mm thick slices, and 8 mm disks were punch cut from the tissue using a dermal punch. The samples were soaked in 0.1 M $FeCl_3$ solution for 2 h in the dark. Samples were irradiated using a 405 nm LED lamp (Thorlabs). The intensity of light at the surface of the specimen (irradiance) was 145 mW cm^{-2}, as measured with a S121C photodiode power sensor (Thorlabs). A series of iron-containing samples was kept always in the dark and used as a thermal control. Elastic moduli were measured using a TA instruments Discovery HR-2 rheometer using 8 mm parallel plate geometry. The samples were compressed at 1 Hz with an axial strain of 5%, at 25.0 °C. Fe(III)-containing parsnip specimens were measured immediately after stopping the irradiation experiments.

3 Results and discussion

3.1 Fe(III)-Polysaccharide photochemical radical generation

To determine the identity of the radical generated in the photolysis of Fe(III)-polyuronic acid systems, the radical spin trap 5,5-dimethyl-1-pyrroline N-oxide (DMPO) was used with the polyuronic acid alginate. The EPR spectra of Fe(III)-alginate with DMPO showed no signal in the initial analysis before the irradiation process which indicated that no photoreduction had taken place on the coordinated polyuronic acid under dark conditions (Fig. 1a). After an irradiation into the observed LMCT band (Fig. S3) with a 405 nm light source for 60 s, a six peak EPR signal was observed. Computer simulation of the spectra (Fig. 1b) was obtained and the hyperfine splittings measured: A_N and $A_{H\beta}$ were 15.4 Gauss and 18.5 gauss respectively for a DMPO spin adduct. The hyperfine splitting corresponds to the generation of a carbon (IV) oxide anion radical ($CO_2^{\bullet-}$) as confirmed by the NIH spin trap database.[32] Previous works have reported similar spectra from the trapping of this radical [21, 22, 33–35]. The rotational correlation time

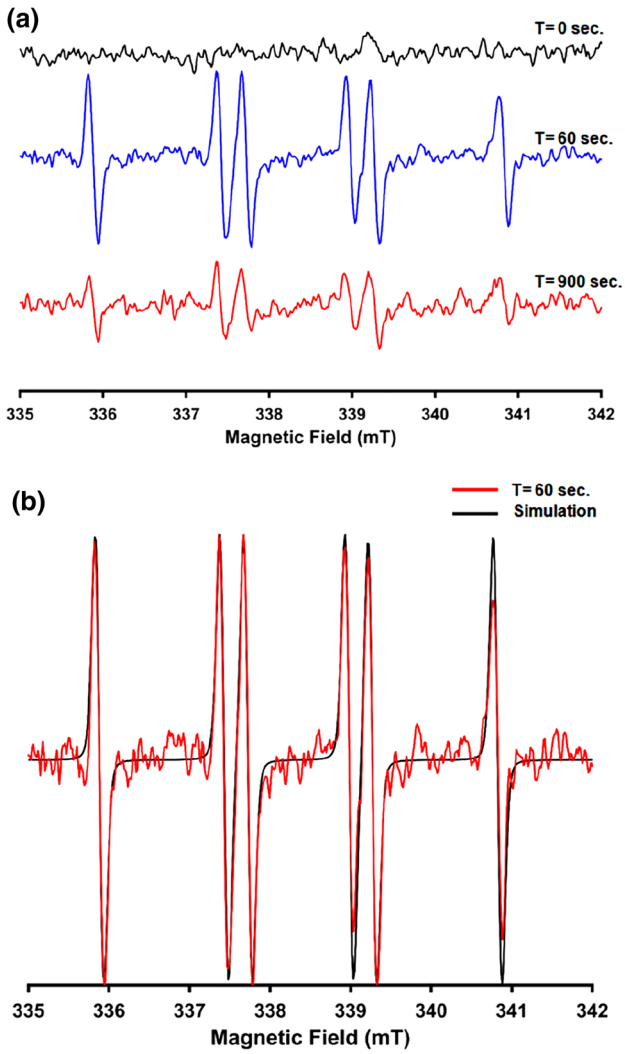

Fig. 1 **a** Spin trapping experiment of photolyzed Alginate M with 405 nm light source at different time intervals. **b** EPR spectra simulation of photolyzed alginate after 60 s

of the spin adduct was also calculated to be 1.682 ns. This correlation time of the spin adduct in aqueous solution tends to be higher than what is usually expected with small moiety trapped radicals because of the slightly higher viscosity of the polysaccharide solution as indicated earlier during the preparation step. Continuous photolysis after 900 s showed a decay of the EPR signal (Fig. 1a). This is indicative of the instability of the spin adduct under prolonged photolysis. This can be ascribed to the formation of much more reactive and unstable aminyl radical derivative from the nitroxide spin adduct which is produced via intermolecular nitronyl O–atom abstraction under further photolysis as shown in Scheme S1 [34].

The lifetime of the spin adduct was slightly longer after 900 s photolysis when the light source was changed to a 390 nm LED lamp with similar intensity (Fig. S4). Similarly,

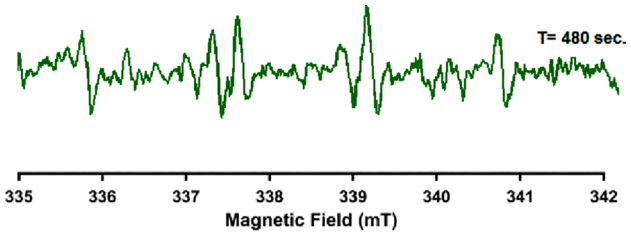

Fig. 2 Results of a spin trapping experiment during photolysis of the Fe(III)-pectate system using 405 nm light source

EPR spectra of Fe(III)-pectate showed signals for spin trapped adduct corresponding to $CO_2^{\bullet-}$ radical generation after photolysis for 480 s, which rapidly decayed away (Fig. 2). These results implicate pathway B from Scheme 1, as the photochemical pathway observed in the Fe(III)-polyuronic acid systems, where bond cleavage of the carboxylate leads to generation of the free $CO_2^{\bullet-}$ which can be stabilized by the iron ions nearby due to the bent geometry. Unlike in Fe(III) α-hydroxy acid systems, where CO_2 generation is observed after ligand to metal charge transfer followed by homolytic bond cleavage as in pathway A, in this alternative pathway the generation of the radical occurs before ligand to metal charge transfer, and additional reaction of the [Fe(II)–$COO^{\bullet}$] radical intermediate to form CO_2 is not needed. It should be noted, that in the solid state, CO_2 generation was observed for the Fe(III)-alginate system, but it was never quantified, and in solution no gas bubbles have been observed [19]. It is likely then, that for the polyuronic acid systems in aqueous gels pathway B predominates, and in the solid state, entropic effects could favor pathway A.

3.2 Scope of Fe(III)-Polyuronic acid photochemistry

In order to show the scope of the Fe(III)-polyuronate photochemistry in natural polysaccharide systems, the efficiency of the photochemical reaction of different polysaccharides was evaluated by quantitatively measuring the amount of Fe(II) produced upon irradiation with light (405 nm, 50 mW cm^{-2}). The results presented in Table 1 show the quantum yields ($\Phi_{Fe(II)}$) for the photoreduction of Fe(III) in the various uronate-containing polysaccharide samples. For all of the polyuronic-acid contacting polysaccharides that we investigated, a photochemical reaction was observed, even for an isolated pectic polysaccharide from Noni fruits and potato starch that had been oxidized to have some glucuronic acid content (Table 1).

The fourfold dilution of the Fe(III)-polysaccharide solution resulted in a decrease in the photochemical quantum yield (QY) for all systems. It is important to note that, although the polysaccharide concentration expressed in w/v % did not necessarily yield the same Fe(III) to uronate

Table 1 Quantum yields, ($\Phi_{Fe(II)}$ (± standard deviation, ± SD) for the photoreduction of Fe(III) for different polysaccharide systems at two different concentrations

Sample	$(\Phi_{Fe(II)} \pm SD) \times 10^2$		% of Uronate monomer found in polymer
	1% PS/ 0.9 mM Fe(III)	0.25% /0.23 mM Fe(III)	
Alginate 35% M (AlgG)	1.8 ± 0.4	0.145 ± 0.007	100
Alginate 61% M (AlgI)	3.80 ± 0.04	0.58 ± 0.02	100
Alginate 65%M (AlgM)	10.9 ± 0.5	9.4 ± 0.3	100
Pectin	2.7 ± 0.1	1.5 ± 0.1	74
Pectate (Pect)	1.7 ± 0.1	0.66 ± 0.03	100
Xanthan Gum (Xant)	–	0.11 ± 0.02	20
Gum Arabic (GA)	1.1 ± 0.2	0.9 ± 0.1	12–20
Noni	–	1.4 ± 0.4	62
Hyaluronic acid	0.3 ± 0.4	0.036 ± 0.006	50
Oxidized Starch (OS)	1.7 ± 0.1	0.9 ± 0.3	82

The amount of Fe(III) per gram of polysaccharide was kept constant for all systems

molar ratio for all systems, it did for polysaccharides with the same uronate content such as AlgG, AlgI, AlgM, and Pectate (~ 56:1 iron-to-carboxylate). Interestingly, the concentration effect was very important for some systems such as AlgG, for which the yield was 92% lower after dilution, while it did not have the same effect for systems such as AlgM, which was only 14% lower (Table 1). Focusing on the 0.25% alginate solutions we observed that the QY for the different alginate systems trended with the mannuronate content, consistent with what was previously observed for Fe(III)-alginate systems at a higher concentration [36]. Furthermore, regardless of the concentration of the solution, the highest quantum yield of the series was observed for AlgM, and the lowest one was observed for hyaluronic acid. The different values of QY within the same family of uronic acids indicated that epimeric composition was not the most important factor. The quantum yields also did not trend with the carboxylate content (e.g., pectin, with only 74% free uronates was more reactive than pectate, with 100% uronate content). Based on these and previous results, we suggest that these differences in quantum yield were due to differences in the interaction of the polysaccharide with Fe(III) ions, where changes in the polysaccharide structure, as well as Fe(III) concentrations affects the type of coordination in the solutions. We previously showed by Mossbauer spectra, that there were differences in the Fe(III) species when the Fe(III)-AlgM gels were compared to the Fe(III)-pectate gels [25]. The dominant iron species detected in both the alginate and pectate hydrogels was Fe(III)-oxo hydroxo nanoclusters [25]. There were differences, however, in the overall speciation of alginate vs. pectate gels, where alginate gels showed 60% Fe(III) oxo hydroxo nanoclusters and 20% Fe(III)-hydroxo carboxylate bridged dimers [25]. The pectate gels showed 80% Fe(III) oxo hydroxo nanoclusters and only 5% Fe(III)-hydroxo carboxylate bridged dimers.

This suggests that differences in the QY can be explained by changes in the Fe(III) speciation, where the speciation affects the overall stability of the radical. For example, the Fe(III)-hydroxo carboxylate dimer could stabilize the carboxylate for bond cleavage, and therefore stabilize formation of the $CO_2^{\bullet-}$ radical. The greater dimer coordination in the more photoactive alginate with 65% M compared to pectate could account for the changes in the quantum yield.

To determine how the assembly of the polysaccharides was affected by the photoreaction, and quantify the breakdown of the polymer chain, the Fe(III)-polysaccharide solutions were analyzed by dynamic light scattering (DLS). A clear and systematic decrease in the hydrodynamic radius (R_h) of the Fe(III)-polysaccharide assemblies was observed upon irradiation (Fig. S5). All systems behaved similarly. They all had a sharp initial drop in the particle size that reached a plateau (Fig. S5). The decrease in R_h was attributed to the decrease in molecular weight of the polysaccharide, due to subsequent reaction after the radical generation (Scheme 1). This molecular weight decrease was due to the breakdown of the polysaccharide backbone to form more stable products from the more unstable aldehyde upon generation of the carbon (IV) oxide anion radical $CO_2^{\bullet-}$ (Scheme1). In addition, the loss of carboxylate groups as $CO_2^{\bullet-}$ during the photoreaction also contributed to an increase in hydrophobicity of the polyuronic acids which can change how the Fe(III)-coordination affects the overall assembly of the polysaccharides in solution [37].

Using the change in hydrodynamic radius after 60 s irradiations (ΔR_h/min), we compared the rate of photo degradation of the aggregates for the different polysaccharides. The rate of decomposition for all the evaluated systems trends with the quantum yield of photoreduction of Fe(III) (Fig. 3). This suggests that changes in Fe(III)-speciation and polymer assembly correlated with the QY, and thus the degradation of the Fe(III)-polysaccharide assemblies depended on the

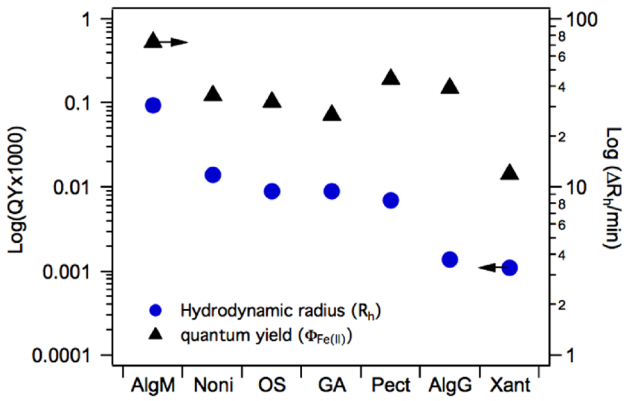

Fig. 3 Change of hydrodynamic radius (R_h) of Fe(III)-polysaccharide suspensions after irradiation (blue circles) with 405 nm light (50 mW) for 60 min compared to the QY for the different polysaccharides (black triangles)

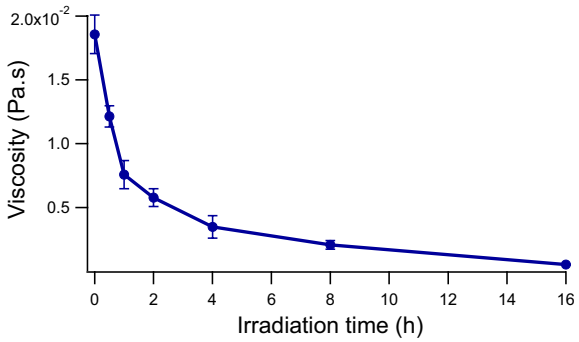

Fig. 4 Change of viscosity upon irradiation with 405 nm LED (50 mW cm^{-2}) for 0.9 mM Fe(III) 1% Alg I solutions

photoreaction. The degradation of the polysaccharides was also quantified using oscillatory rheology to look at viscosity changes. As expected, a decrease in viscosity of the solution was observed with increasing irradiation time, indicating a drop in the molecular weight of the alginate after irradiation (Fig. 4).

3.3 Fe(III)-polysaccharide photochemistry in natural materials

Many natural materials contain high amounts of uronic acid-containing polysaccharides like pectins, and Carrano and co-workers have shown that these polysaccharides are involved in Fe(III) coordination in marine plants similarly to the Fe(III)-alginate [5, 6, 25]. We wanted to investigate the Fe(III)-carboxylate photochemistry in these materials. For an example biomaterial scaffold, we chose Parsnip (*Pastinaca sativa*), which has a uronic acid content as high as 10% (dry basis) and little natural pigment or chromophores to interfere with the photochemistry [38]. These parsnip materials were soaked in 0.1 M $FeCl_3$ to ensure Fe(III) coordination, and irradiated. Electron Microscopy of the parsnip materials showed that irradiation caused a noticeable disorganization of the cellular structure (Fig. 5a, b and), while keeping a rather defined structure for each individual cell (Fig. S6a, b). These results suggested a primary degradation of the middle lamella, where high pectin (polyuronic acid) content is known to be important in cementing adjacent cell walls together [39, 40].

Observation of the irradiated plant tissue before treating the sample with EDTA (Fe(III)/Fe(II) present) indicated a clear separation of the cell walls previous to the removal of the iron (Fig. S6c), proving that the observed changes were due to the irradiation process and not to the effect of Fe(III) chelating. Mechanical testing of the Fe(III)-loaded parsnip tissue indicated a systematic weakening of the cellular structure as the material was exposed to 405 nm LED light. The observed drop in elastic modulus confirms the photo degradation of the studied pectin-rich tissue, corresponding to breakdown of the pectin chain (Fig. 5c). Our results indicated that the photochemistry of Fe(III)-polyuronates occurred not only in isolated and purified

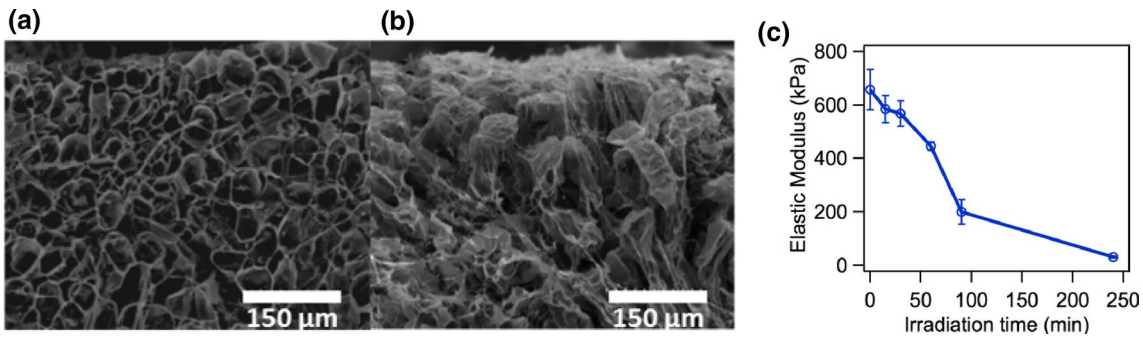

Fig. 5 SEM Image of 2 mm thick parsnip tissues soaked in 0.1 M $FeCl_3$ for 2 h in dark **a** before and **b** after irradiation with 405 nm LED (145 mW cm^{-2}) **c** changes in elastic modulus (E') with irradiation time for Fe(III)-parsnip root tissue

uronate-containing polysaccharide solutions, but also in natural pectin-containing materials in plants. These results highlight that Fe(III)-polyuronic acid photochemistry can indeed play a role in biogeochemical iron cycling in soil via root tissues, and can be one mechanism responsible for degradation of the plant material.

4 Conclusions

The Fe(III)-polyuronic acids are photoactive, and the photoreaction proceeds through two possible pathways that with generation of the $CO_2^{\bullet-}$ radical (Pathway B) or Fe(II) and oxidative decarboxylation (Pathway A), with breakdown of the polysaccharide chain into, smaller assemblies and less viscose materials. The quantum yields for the photoreduction of Fe(III) were measured for a series of natural and synthetically modified uronate-containing polysaccharides in solution at two different concentrations. All the studied polysaccharide systems were able to reduce ferric ions under 405 nm LED light irradiation. The quantum yields were different depending on the specific polysaccharide, and these changes were attributed to changes in the Fe(III) coordination, which can stabilize the homolytic bond cleavage leading to a more efficient generation of the radical $CO_2^{\bullet-}$ photoproduct (Pathway B) compared to LMCT with Fe(II) generation and subsequent oxidative decarboxylation (Pathway A). Our results show that this photoreaction can occur in plant tissues in the presence of Fe(III), and in polysaccharide hydrogels coordinated with Fe(III). Although our results present only degradation of the polyuronic-acid containing natural materials, we envision more advanced experiments such as the patterning of the materials with light, or even the use of the other radical reactive species to further modify and change the surface chemistry as the material is irradiated. This work also highlights the importance of the inorganic components in natural systems, and how such Fe(III)-polyuronic acid photochemistry can contribute to biogeochemical cycling of iron.

Supplementary Information The online version contains supplementary material available at https://doi.org/10.1007/s43630-021-00014-0.

Acknowledgements This work was partially supported by Bowling Green State University through start-up funds. We also thank Dr. Marilyn Cayer at the Bowling Green State University Department of Life Sciences SEM Center

Author contributions The manuscript was written through contributions of all authors. All authors have given approval to the final version of the manuscript.

Funding ADO thanks the NSF CAREER award, Division of Chemistry, Chemical Structure, Dynamics and Mechanisms- B Program and Division of Materials Research Polymers program (CHE-1653892) for support of this work. MDEF thanks the National Science Foundation for continued support of his research through grant # CHE–1900541.

Data availability All data generated or analyzed during this study are included in this published article [and its supplementary information files]. Additional raw data can be obtained via the corresponding author.

Code availability Not applicable.

Compliance with ethical standards

Conflict of interest There are no conflicts to declare.

References

1. Amin, A. S., Green, H. D., Küpper, C. F., & Carrano, J. C. (2009). Vibrioferrin, an unusual marine siderophore: iron binding, photochemistry, and biological implications. *Inorganic Chemistry, 48*(23), 11451–11458.
2. Barbeau, K., Rue, E. L., Bruland, K. W., & Butler, A. (2001). Photochemical cycling of iron in the surface ocean mediated by microbial iron(iii)-binding ligands. *Nature, 413*(6854), 409–413.
3. Butler, A., & Theisen, R. M. (2010). Iron(III)-siderophore coordination chemistry: Reactivity of marine siderophores. *Coordination Chemistry Reviews, 254*(3–4), 288–296.
4. Hardy, C. D., & Butler, A. (2018). β-Hydroxyaspartic acid in siderophores: biosynthesis and reactivity. *Journal of Biological Inorganic Chemistry, 23*(7), 957–967.
5. Miller, E. P., Böttger, L. H., Weerasinghe, A. J., Crumbliss, A. L., Matzanke, B. F., Meyer-Klaucke, W., et al. (2014). Surface-bound iron: a metal ion buffer in the marine brown alga *Ectocarpus siliculosus*? *Journal of Experimental Botany, 65*(2), 585–594.
6. Miller, E. P., Auerbach, H., Schünemann, V., Tymon, T., & Carrano, C. J. (2016). Surface binding, localization and storage of iron in the giant kelp *Macrocystis pyrifera*. *Metallomics, 8*(4), 403–411.
7. Barbeau, K., Rue, E. L., Trick, C. G., Bruland, K. W., & Butler, A. (2003). Photochemical reactivity of siderophores produced by marine heterotrophic bacteria and cyanobacteria based on characteristic Fe(III) binding groups. *Limnologu Oceanography, 48*(3), 1069–1078.
8. Abrahamson, H. B., Rezvani, A. B., & Brushmiller, J. G. (1994). Photochemical and spectroscopic studies of complexes, of iron(III) with citric acid and other carboxylic acids. *Inorganica Chim Acta, 226*(1), 117–127.
9. Waite, T. D., & Morel, F. M. M. (1984). Photoreductive dissolution of colloidal iron oxide: Effect of citrate. *Journal of Colloid and Interface Science, 102*(1), 121–137.
10. Zuo, Y., & Hoigné, J. (1994). Photochemical decomposition of oxalic, glyoxalic and pyruvic acid catalysed by iron in atmospheric waters. *Atmospheric Environment, 28*(7), 1231–1239.
11. Faust, B. C., & Zepp, R. G. (1993). Photochemistry of aqueous iron(III)-polycarboxylate complexes: roles in the chemistry of atmospheric and surface waters. *Environmental Science and Technology, 27*(12), 2517–2522.
12. Glebov, E. M., Pozdnyakov, I. P., Grivin, V. P., Plyusnin, V. F., Zhang, X., Wu, F., et al. (2011). Intermediates in photochemistry of Fe(III) complexes with carboxylic acids in aqueous solutions. *Photochemical and Photobiological Sciences, 10*(3), 425–430.

13. Weller, C., Horn, S., & Herrmann, H. (2013). Photolysis of Fe(III) carboxylato complexes: Fe(II) quantum yields and reaction mechanisms. *Journal of Photochemistry Photobiology Chemistry, 15*(268), 24–36.
14. Borer, P., & Hug, S. J. (2014). Photo-redox reactions of dicarboxylates and α-hydroxydicarboxylates at the surface of Fe(III)(hydr) oxides followed with in situ ATR-FTIR spectroscopy. *Journal of Colloid and Interface Science, 15*(416), 44–53.
15. Kumarathilaka, P., Seneweera, S., Meharg, A., & Bundschuh, J. (2018). Arsenic speciation dynamics in paddy rice soil-water environment: sources, physico-chemical, and biological factors: a review. *Water Research, 1*(140), 403–414.
16. Brummett, A. E., & Dey, M. (2016). New mechanistic insight from substrate- and product-bound structures of the metal-dependent dimethylsulfoniopropionate lyase DddQ. *Biochemistry, 55*(44), 6162–6174.
17. Amin, S. A., Green, D. H., Hart, M. C., Küpper, F. C., Sunda, W. G., & Carrano, C. J. (2009). Photolysis of iron-siderophore chelates promotes bacterial-algal mutualism. *Proceedings of the National Academy of Sciences USA, 106*(40), 17071–17076.
18. Lueder, U., Jørgensen, B. B., Kappler, A., & Schmidt, C. (2020). Photochemistry of iron in aquatic environments. *Environ Sci Process Impacts, 22*(1), 12–24.
19. Giammanco, G. E., Sosnofsky, C. T., & Ostrowski, A. D. (2015). Light-responsive iron(III)–polysaccharide coordination hydrogels for controlled delivery. *ACS Applied Materials and Interfaces, 7*(5), 3068–3076.
20. Pozdnyakov, I. P., Melnikov, A. A., Tkachenko, N., Chekalin, S. V., Lemmetyinen, H., & Plyusnin, V. F. (2014). Ultrafast photophysical processes for Fe(III)-carboxylates. *Dalton Transactions, 43*(47), 17590–17595.
21. Mangiante, D. M., Schaller, D. R., Zarzycki, P., Banfield, F. J., & Gilbert, B. (2017). Mechanism of ferric oxalate photolysis. *ACS Earth and Space Chemistry, 1*(5), 270–276.
22. Jeong, J., & Yoon, J. (2004). Dual roles of CO_2^- for degrading synthetic organic chemicals in the photo/ferrioxalate system. *Water Research, 38*(16), 3531–3540.
23. Chen, J., & Browne, W. R. (2018). Photochemistry of iron complexes. *Coordination Chemistry Reviews, 1*(374), 15–35.
24. Šima, J., & Makáňová, J. (1997). Photochemistry of iron (III) complexes. *Coordination Chemistry Reviews, 1*(160), 161–189.
25. Auerbach, H., Giammanco, G. E., Schünemann, V., Ostrowski, A. D., & Carrano, C. J. (2017). Mössbauer spectroscopic characterization of iron(III)–polysaccharide coordination complexes: photochemistry, biological, and photoresponsive materials implications. *Inorganic Chemistry, 56*(19), 11524–11531.
26. Deiana, S., Premoli, A., Senette, C., Gessa, C., & Marzadori, C. (2003). Role of uronic acid polymers on the availability of iron to plants. *Journal of Plant Nutrition, 26*(10–11), 1927–1941.
27. Deiana, S., Palma, A., Premoli, A., & Senette, C. (2007). Possible role of the polyuronic components in accumulation and mobilization of iron and phosphate at the soil–root interface. *Iron Nutrition Interaction Plants., 45*(5), 341–349.
28. Stoll, S., & Schweiger, A. (2006). EasySpin, a comprehensive software package for spectral simulation and analysis in EPR. *Journal of Magnetic Resonance, 178*(1), 42–55.
29. Bui, A. K. T., Bacic, A., & Pettolino, F. (2006). Polysaccharide composition of the fruit juice of *Morinda citrifolia* (Noni). *Phytochemistry, 67*(12), 1271–1275.
30. Kuhn, H. J., Braslavsky, S. E., & Schmidt, R. (1989). Chemical actinometry. *Pure and Applied Chemistry, 61*(2), 187–210.
31. Morris, E. R., Rees, D. A., & Thom, D. (1980). Characterisation of alginate composition and block-structure by circular dichroism. *Carbohydrate Research, 81*(2), 305–314.
32. NIH Spin Trap Database. (2021). https://tools.niehs.nih.gov/stdb/. Accessed 12 Nov 2020
33. Harbour, J. R., & Bolton, J. R. (1978). The involvement of the hydroxyl radical in the destructive photooxidation of chlorophylls in vivo and in vitro. *Photochemistry and Photobiology, 28*(2), 231–234.
34. Villamena, A. F., Locigno, J. E., Rockenbauer, A., Hadad, M. C., & Zweier, L. J. (2006). Theoretical and experimental studies of the spin trapping of inorganic radicals by 5,5-dimethyl-1-pyrroline n-oxide (DMPO). 2. Carbonate radical anion. *The Journal of Physical Chemistry A, 111*(2), 384–391.
35. Villamena, F. A., Locigno, E. J., Rockenbauer, A., Hadad, C. M., & Zweier, J. L. (2006). Theoretical and experimental studies of the spin trapping of inorganic radicals by 5,5-dimethyl-1-pyrroline n-oxide (DMPO). 1. Carbon dioxide radical anion. *The Journal of Physical Chemistry A, 110*(49), 13253–13258.
36. Giammanco, E. G., & Ostrowski, D. A. (2015). Photopatterning the mechanical properties of polysaccharide-containing gels Using Fe3+ coordination. *Chemistry of Materials, 27*(14), 4922–4925.
37. Okajima, K. M., Nguyen, T. Q., Tateyama, S., Masuyama, H., Tanaka, T., Mitsumata, T., et al. (2012). Photoshrinkage in polysaccharide gels with trivalent metal ions. *Biomacromolecules, 13*(12), 4158–4163.
38. Castro, A., Bergenståhl, B., & Tornberg, E. (2012). Parsnip (*Pastinaca sativa* L.): Dietary fibre composition and physicochemical characterization of its homogenized suspensions. *Food Research International, 48*(2), 598–608.
39. Albersheim, P., Muhlethaler, K., & Frey-Wyssling, A. (1960). Stained pectin as seen in the electron microscope. *The Journal of Biophysical and Biochemical Cytology, 8*(2), 501–506.
40. Mohnen, D. (2008). Pectin structure and biosynthesis. *Current Opinion in Plant Biology, 11*(3), 266–277.

Authors and Affiliations

M. H. Jayan S. Karunarathna[1] · Mayokun J. Ayodele[1] · Giuseppe E. Giammanco[1] · Alexander M. Brugh[1] · Dayana A. Muizzi[1] · Mariia A. Bauman[1] · Andrew T. Torelli[1,3] · Anginelle M. Alabanza[2] · Malcolm D. E. Forbes[1,2] · Alexis D. Ostrowski[1]

[1] Department of Chemistry and Center for Photochemical Sciences, Bowling Green State University, Bowling Green, OH 43403, USA

[2] Department of Chemistry, University of North Carolina, Chapel Hill, NC, USA

[3] Present Address: Department of Chemistry, Ithaca College, Ithaca, NY 14850, USA